

Numerical study on combed teeth serrations for wind turbine noise reduction

van der Velden, Wouter; Oerlemans, Stefan

DOI

[10.2514/6.2017-4172](https://doi.org/10.2514/6.2017-4172)

Publication date

2017

Document Version

Accepted author manuscript

Published in

23rd AIAA/CEAS Aeroacoustics Conference

Citation (APA)

van der Velden, W., & Oerlemans, S. (2017). Numerical study on combed teeth serrations for wind turbine noise reduction. In *23rd AIAA/CEAS Aeroacoustics Conference: 5-9 June 2017, Denver, Colorado* Article AIAA 2017-4172 American Institute of Aeronautics and Astronautics Inc. (AIAA).
<https://doi.org/10.2514/6.2017-4172>

Important note

To cite this publication, please use the final published version (if applicable).
Please check the document version above.

Copyright

Other than for strictly personal use, it is not permitted to download, forward or distribute the text or part of it, without the consent of the author(s) and/or copyright holder(s), unless the work is under an open content license such as Creative Commons.

Takedown policy

Please contact us and provide details if you believe this document breaches copyrights.
We will remove access to the work immediately and investigate your claim.

Numerical study on combed teeth serrations for wind turbine noise reduction

W.C.P. van der Velden*

Delft University of Technology, Kluyverweg 1, 2629 HS, Delft, the Netherlands

S. Oerlemans†

Siemens Wind Power, Borupvej 16, 7330, Brande, Denmark

This study investigates the flow topology and noise emission from a wind turbine airfoil with combed serration trailing edge geometry, to understand the noise reduction observed in earlier experiments. A comparison is made to a straight trailing edge and a serrated trailing edge without combs. The different trailing edges are retrofitted to a cambered airfoil at design angle of attack. The flow field is analyzed by evaluating the fully explicit, transient, compressible Lattice Boltzmann equation. The acoustic far field is obtained by means of the Ffowcs-Williams and Hawkings integral solution, Curle's integral solution, and a direct probe solution. The simulated mean pressure distribution matches earlier wind tunnel experiments (obtained from the Virginia Tech anechoic facility) well. Furthermore, the numerical results confirm that the combed serrations give a larger noise reduction than the standard serration. Both trailing edge geometries show similar acoustic trends as the experiments, giving confidence in the numerical results.

I. Introduction

Wind energy; the solution to deal with an increasingly recognized and critical challenge for mankind. In order to reduce greenhouse gases, the demand for renewable energy, such as wind energy, is growing and growing. A study from van den Berg¹ showed that noise, and especially the swishing character of the noise, is one of the most annoying aspects of onshore wind turbines. To protect public health, governments apply strict noise regulations for both maximum, average and modulated noise levels for wind turbines.² Hence, noise constitutes an important barrier for the widespread application of wind energy³ as many wind turbines must operate at reduced power, especially during the night. This leads to a lower power output from the turbines, which will lead to an overall reduction of the annual energy production, finally resulting in loss of revenue.

For a modern large wind turbine, aerodynamic noise from the blades is generally considered to be the dominant noise source, provided that mechanical noise is adequately treated.^{4,5} Most aerodynamic blade noise sources, such as tip noise and blunt-trailing-edge noise, can be prevented by good design. Nevertheless, it is now widely accepted that turbulent-boundary-layer-trailing edge noise (subsequently denoted as trailing edge noise) is the dominant noise source for modern large wind turbines.^{6,7} The trailing edge noise from a well-designed blade with attached flow and a thin trailing edge is relatively low compared to other objects moving at the same speeds. Many passive mitigation strategies have been proposed to further reduce this source of noise. The most successful concept are serrations. Acoustic measurements carried out in wind tunnels and in-field, reported that sawtooth trailing edge serrations offer the most effective noise reduction, also taking into account the simplicity of the design.⁸⁻¹⁵ Far-field noise reductions with respect to the straight trailing edge configuration, expressed as differences in Sound Pressure Level (SPL), of approximately 7 dB and 3 dB, were respectively measured in wind tunnels and in-field applications by previous mentioned authors. Although serrations are now used quite often on the outer part of wind turbine blades, the noise

*Currently Senior Aerospace Application Engineer at Exa GmbH, Stuttgart, Germany, wouter@exa.com

†Senior Key Expert Aeroacoustics

reduction mechanism is not fully understood. Therefore, understanding and modeling the physics associated with the generation and propagation of noise is of paramount importance for the design of more silent wind turbines.

As described analytically by Howe,^{16,17} serrations can reduce trailing edge noise due to the acoustic diffraction effect; however, measured noise reductions are usually much smaller than predicted by theory. Furthermore, aerodynamic effects may also influence the acoustic performance of serrations,^{11,14,18–21} indicating the complexity when adding serrations to trailing edges.

Recent research from Oerlemans⁵ revealed various optimization studies, carried out at Siemens Wind Power (SWP) in the past. Several parameters, such as tooth length, angle and aspect ratio, were systematically varied and tested in acoustic wind tunnel and field measurements. The study presented a novel concept; the combed serration, which proved substantial extra noise reductions over the more conventional serrated designs. Wind tunnel and full-scale field measurements on the new concept, further denoted the combed serration, demonstrated that there is further noise reduction potential beyond optimized serrations. To fully understand the working principle behind the extra noise reductions due to the combs between the teeth, a numerical study was performed by van der Velden and Oerlemans.²¹ The combed teeth were retrofitted to a symmetric NACA 0018 airfoil at zero lift configuration. Multiple analyses were performed on the numerical data, such as an investigation of the effect of the combed teeth on the acoustic directivity, mean and fluctuating flow velocity, boundary layer characteristics, convection velocity, wall pressure fluctuations and spanwise coherence. It was found that the streamlines were more aligned with the serrated edge due to inclusion of the combs, thereby effectively reducing the efficiency of the scattering of noise.^{16,17} However, the effects on a cambered and loaded airfoil, under realistic Reynolds numbers for wind turbine purposes, were not investigated.

This report addresses the gap between what is currently available in literature, and what is aimed for in industry. The flow field and noise emission around a Siemens designed wind turbine airfoil with conventional and novel serrations, subsequently denoted as serration and combed serration, is determined. The flow and pressure field is analyzed by evaluating the fully explicit, transient, compressible Lattice Boltzmann equation. Acoustic perturbations are directly obtained in the numerical domain, enabling analysis of the actual noise reduction mechanism in close comparison with earlier studies. The far field acoustic data is obtained by means of a Ffowcs-Williams and Hawkins²² and Curle²³ integral solution, and is compared against acoustic array data obtained from wind tunnel campaigns performed by SWP in the anechoic wind tunnel of Virginia Tech. A similar computational methodology has been validated against experiments obtained from the anechoic facility in Notre Dame University before, as presented by van der Velden et al.²⁴ for trailing edge noise cases, and is extended in the current study to the incorporation of noise-suppression add-ons at Reynolds numbers larger than 1 million.

II. Computational methodology

The commercial software package Exa PowerFLOW 5.3c was used to solve the discrete Lattice-Boltzmann equations for a finite number of directions. To retrieve the Navier-Stokes relations, a third-order truncation of the Chapman-Enskog expansion can be used.²⁵ For a detailed description of the equations used for the source field computations the reader can refer to studies of Succi²⁶ and van der Velden et al.²⁷ Below, a summary will be provided regarding the steps taken in the overall process.

The discretization used for this particular application consists of 19 discrete velocities in three dimensions (known as the D3Q19 model). In practice this means that a group of particles in a three-dimensional space can stream to up to 19 directions in one cell. For three dimensional simulations of low Mach number flow under ideal gas conditions, this is found to well represent the physical flow field.²⁶ The distribution of particles was solved using the kinetic equations on a Cartesian mesh, with the conventional Bhatnagar-Gross-Krook (BGK) collision term operator,²⁸ the only one available within this commercial software package. A Very Large Eddy Simulation (VLES) was implemented as viscosity model to locally adjust the numerical viscosity of the scheme in regions that are under-resolved.²⁹ A sub-grid scale model is essential to obtain solutions of transient high Reynolds flow problems within industrial turn-around times. The model consists of a two-equation $\kappa - \epsilon$ Renormalization Group (RNG) modified to incorporate a swirl based correction that reduces the modeled turbulence in presence of large vortical structures, required for stability of the code. Due to the limitations of the discretization model D3Q19, the cells, further denoted as voxels, are equally sized in each direction. This makes it challenging to perform wall resolved simulations. Hence, a turbulent wall-model

was used to resolve the near-wall region.³⁰ The particular choice of the wall model in combination with the subgrid scale model allows to obtain a reliable estimate of the boundary layer till the viscous sub-layer, well staying within feasible turn-around times.

Due to the fact that the LBM is inherently compressible and it can only provide a time-dependent solution, the acoustic pressure field was extracted directly from the computation domain. Sufficient accuracy is obtained when considering at least 16 lattices per wavelength for the LBM methodology.³¹ The obtained far field noise was further compared with noise estimated by using an acoustic analogy. For this purpose, the FW-H²² equation was employed. The time-domain FW-H formulation developed by Farassat³² was used to predict the far field sound radiation of the serrated trailing edge in a uniformly moving medium.^{31,33} The input to the FW-H solver is the time-dependent pressure field of a porous surface mesh provided by the transient LBM simulations. A simplification was found by employing Curle's²³ analogy, where the surface mesh was fitted to the airfoil surface, commonly used in trailing edge noise predictions.

The distribution in space and frequency of the turbulent flow aeroacoustic sources is visualized by making use of Powell's vortex sound analogy.³⁴ More precisely, the dynamics of the vortical structures can be modeled as a distribution of co-rotating pairs of vortex filaments of length Δl , separated by a distance $2z$, undergoing a rotational motion with angular velocity Ω . Following,³⁵ the total radiated power, emitted by a pair of co-rotating vortices can be estimated as:

$$P_{tot} = \frac{\rho_{\infty} \Delta l \pi^2 \Omega^7 z^7}{8a_0^4}. \quad (1)$$

The Flow Induced Noise Detection (FIND) tool is a post-processing function in PowerACOUSTICS, and is used to detect the individual vortex pairs.

III. Computational setup

A Siemens designed wind turbine airfoil section, modeled with $l = 900$ mm chord, at a design angle of attack, is taken under consideration as baseline model in an undisturbed turbulence free ($< 0.1\%$) flow field at a realistic chord based Reynolds number of $Re_l = 3.3 \cdot 10^6$. Spanwise, cyclic boundary conditions are applied with a modeled span which fits a total of two serrations. Transition is enforced by a zig-zag transition strip just downstream of the leading edge to mimic similar boundary layer trailing edge flow conditions as during the wind tunnel campaign.

A baseline serrated design is tested, as well as an optimized serrated design consisting of a combination of sawtooths and combs; the combed serration. An illustration of the geometry is found in Fig. 1. The dimensions of the sawtooth of the combed serration are similar to the conventional serration. The design tooth flap angle is used for the analysis.

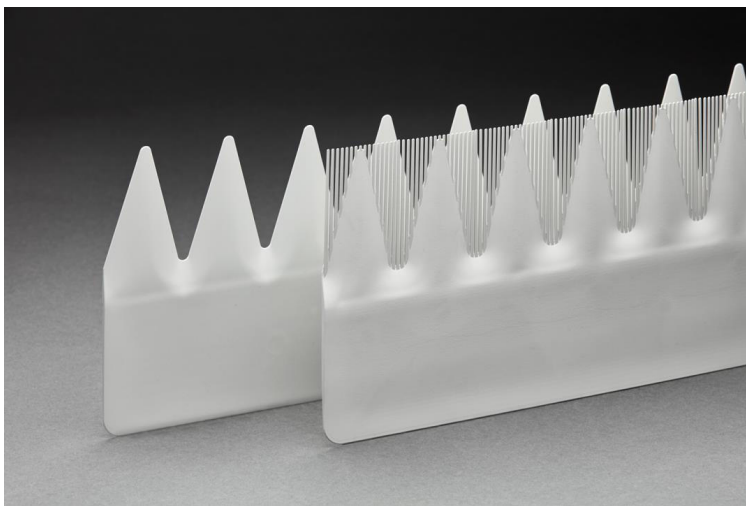


Figure 1. Serration geometry of the conventional and combed serration

The simulation domain size is a block of 10 chords in both streamwise and wall normal direction. Outside

a circular refinement zone of 8 chords diameter, an anechoic outer layer is used to damp acoustic reflections. A total of 9 refinement regions are applied such that, near the boundary of the straight trailing edge (and a box around the serrated edge), the first cell is placed in the lower part of the boundary layer. Smallest voxels are therefore 0.18 mm, which leads to a maximum y^+ at the trailing edge and along the serrated edge of 20. With the coarsest cell being 46 mm, the entire setup leads to approximately 225 million cells. A total of 1.2 million time steps were performed. Performance was measured at 0.58 seconds per timestep on a Linux Xeon E5-2690 2.9 GHz platform of 60 cores.

After the transient phase of approximately 9 flow passes (0.15 sec), sampling is started. The Courant-Friedrichs-Lewy (CFL) number is dependent on the wave propagation velocity and smallest voxel size in this compressible simulation and fixed to unity for each single simulation. Therefore, the physical time step is fixed at $3 \cdot 10^{-7}$ s. Data is sampled at 50 kHz for 0.2 physical seconds at local lattice size, resulting in a recording of 12 flow passes. Fourier transformed data is obtained with a Hamming window with 50 % overlap, to smooth the spectra. Data throughout the paper is presented in 1/3th octave bands, and A-weighted for convenience.

IV. Experimental setup

To validate the computational results, results were taken from a recent aeroacoustic wind tunnel campaign at Virginia's Tech anechoic facility, commissioned by Siemens Wind Power. The same model geometries (both airfoil and serrations) were used as in the computational campaign. A rough sketch of the experimental setup is presented in Fig. 2.

The Virginia Tech Stability Wind Tunnel is a closed loop subsonic wind tunnel with a 1.83×1.83 m rectangular removable test section. The length of the test section is 7.3 m. The tunnel is driven by a 0.45 MW fan of 5.3 m diameter. A flow speed of 75 m/s can be reached in an empty test section. Downstream of the fan, an air exchange tower open to the atmosphere is located. From there the flow is directed into the settling chamber. The settling chamber contains 7 screens with an open area ratio of 0.6 and a separation of 0.15 m. The flow enters the test section through a nozzle with contraction ratio of 9 : 1 and leaves it through a diffuser. All corners of the tunnel are equipped with an array of shaped turning vanes. Turbulence intensities of less than 0.05% were reported from earlier measurements.

Two different test sections are available for the tunnel: a hard wall aerodynamic test section and a acoustic test section with Kevlar walls. For the results presented in this paper, the acoustic test section was used. It has Kevlar side walls designed to contain the flow and keep similar aerodynamic performance as with a closed test section. The acoustic sound waves on the other hand, are transmitted through the walls and can be measured in the anechoic chambers. More details of the acoustic characteristics of the test section can be found in Ref.³⁸

A microphone array consisting of 117 microphones was located in the anechoic chamber. The microphones were arranged in a 9 armed spiral of 13 microphones each, with an overall diameter of 1.1 m. Its location relative to the airfoil is similar to that in Fig. 2. The microphones used in this array are Panasonic model WM-64PNT Electret microphones. These microphones have a flat frequency response from 20 Hz to 16 kHz. All microphones used in the array were calibrated before being installed in the array and selected to be within $\pm 5^\circ$ phase and ± 0.4 dB amplitude from 500 Hz to 16 kHz.

V. Straight trailing edge flow and acoustics assessment

The flow field around the wind turbine airfoil section is depicted in Fig. 3. The flow field undergoes enforced transition due to the zig-zag strip, while the pressure gradient enhances the development of the boundary layer. A fully turbulent boundary layer convects over the trailing edge, interacting with the serrated design. The black line indicates a funnel around the airfoil trailing edge and part of the wake, and is used as porous membrane to sample data for the FW-H acoustic analogy.

Essential in the comparison between experiment and simulation is the proper recording of the flow conditions. Therefore, in a more quantitative manner, the flow and acoustics of the baseline straight trailing edge case is analyzed in Fig. 4. Firstly, the mean pressure distribution is analyzed against experimental data. Overall agreement is good; the numerical result fits the levels and trends of the data obtained in the wind tunnel.

As mentioned in the methodology section, the acoustic far-field spectra (Φ_{aa}) are obtained by three

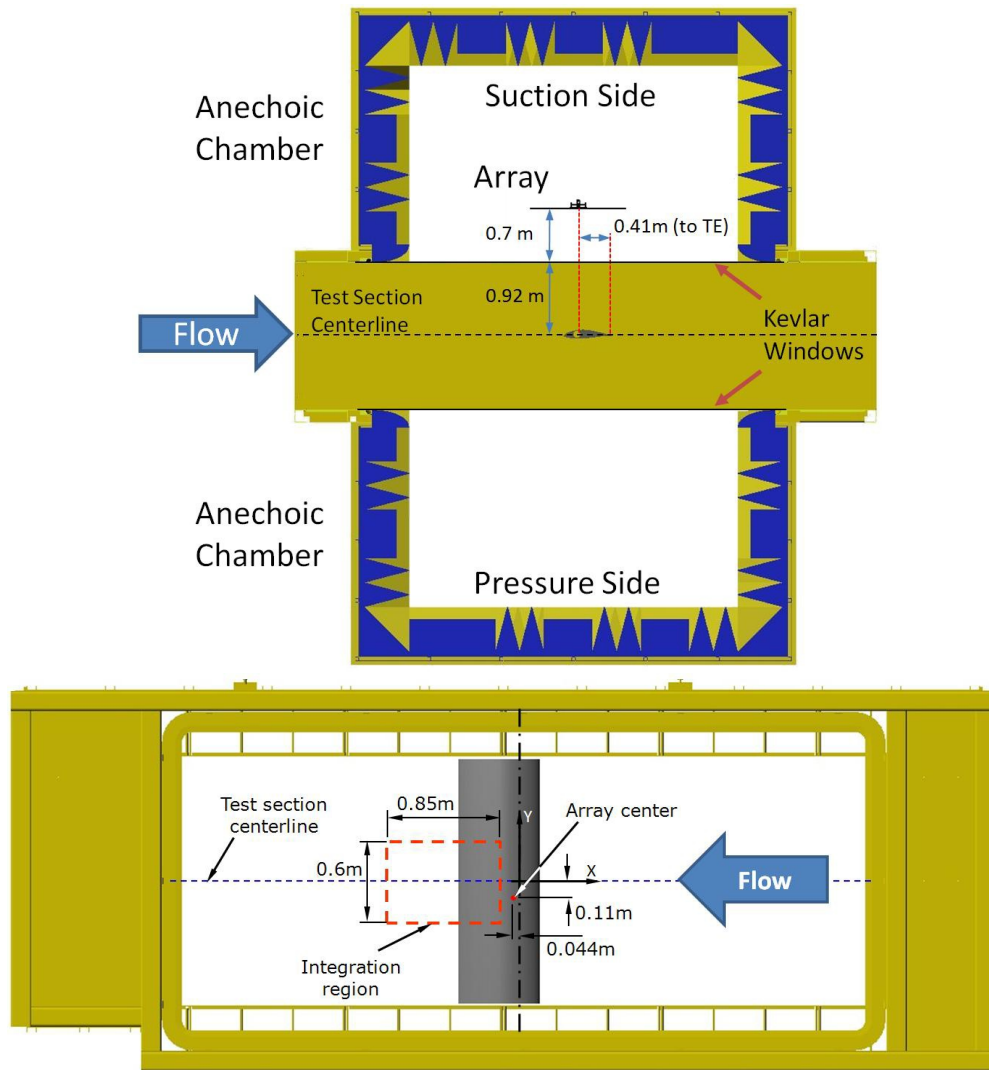


Figure 2. Virginia Tech anechoic test facility setup

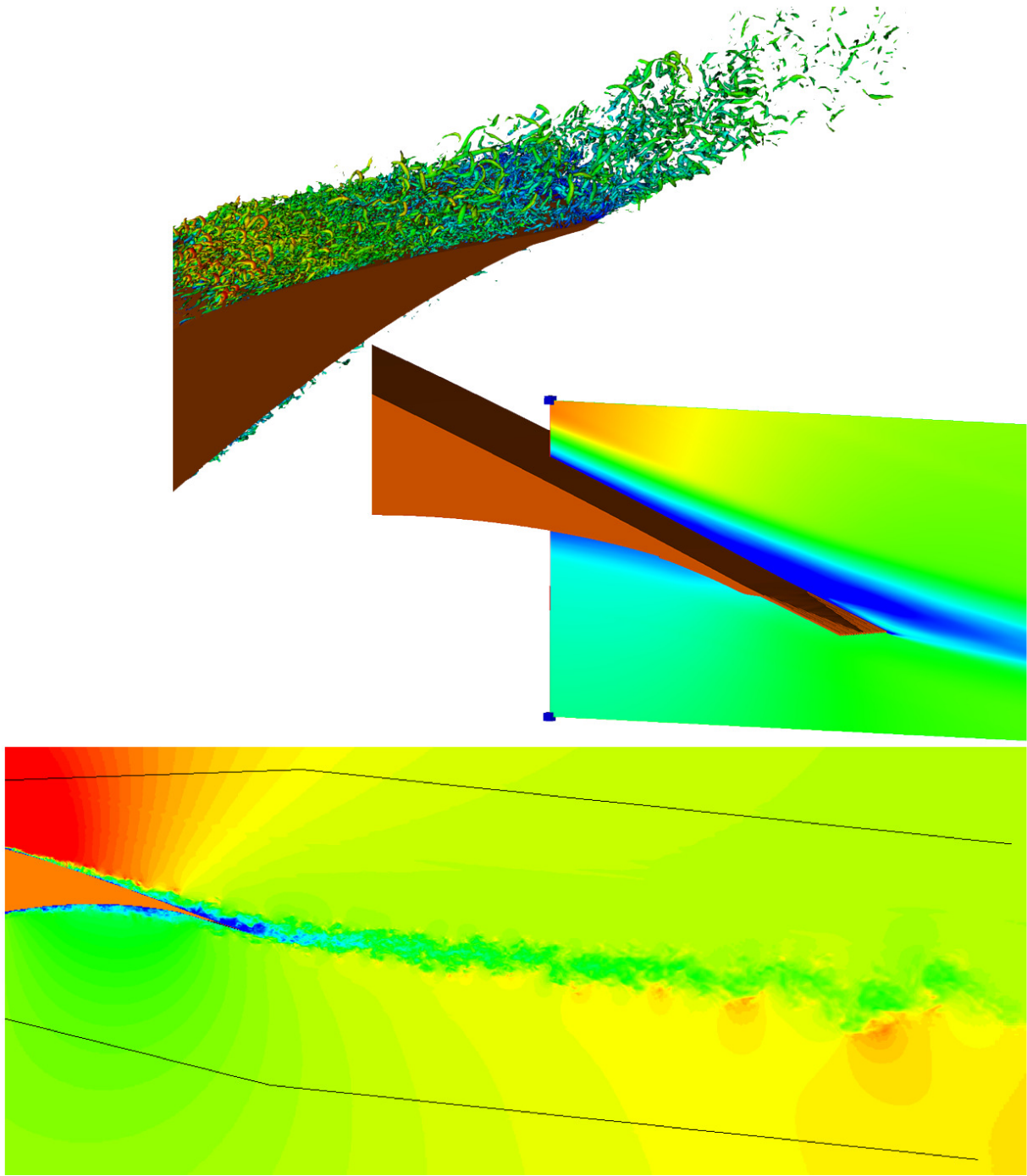


Figure 3. Flow field overview around the trailing edge of the airfoil; iso-surfaces of vorticity (top), mean flow speed magnitude (middle), and instantaneous snapshot of streamwise velocity (bottom).

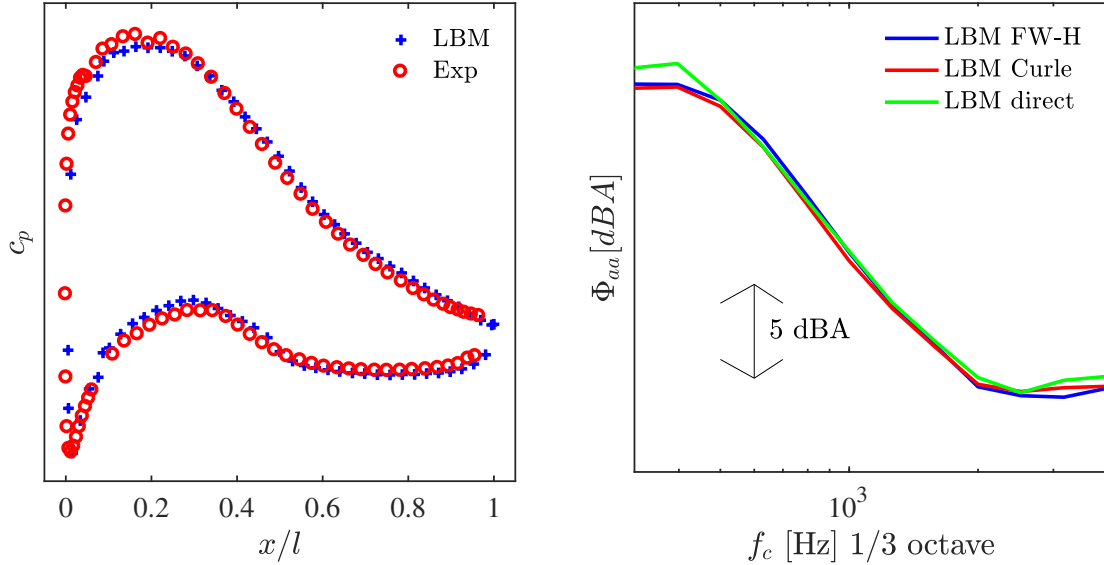


Figure 4. Overview of straight trailing edge results, (left) mean pressure distribution, (right) far field acoustic spectra obtained with different post processing algorithms.

different post-processing methods; 1) directly from a probe in the computational domain, 2) with FW-H analogy using the funnel as source location, 3) with Curle’s analogy using the airfoil surface as source location. To verify that each method gives similar results, they are all plotted for the straight trailing edge case in Fig. 4 (right). Φ_{aa} is the scaled far-field spectrum, obtained as:⁷

$$\Phi_{aa} = \Phi_{meas} + 20 \log_{10}(R_1/R_2) - 10 \log_{10}(b_1/b_2) - 50 \log_{10}(M_1/M_2) \quad (2)$$

Here, index ₂ indicates the reference values with Mach number $M = 1$, observer radius $R = 1$ m and spanwise length $b = 1$ m. The adopted scaling is conventionally used in literature for trailing-edge noise studies, where non-compact noise sources are the most relevant contributions.^{7,36,37} In addition, due to the cyclic boundary conditions and limited span, the acoustic pressure field in the numerical solution contains contributions from mirrored coherent image sources of the airfoil arriving through the cyclic domain boundaries to the microphone location. To correct for this, in addition to the previously mentioned scaling parameters, another correction has to be applied to the sound spectra of the direct probe measurements. Oberai^{39,40} derived a three-dimensional, frequency dependent, correction for low Mach number flows, which can be rewritten in a dB form as $\Phi_{cor} = 10 \log_{10}(fb^2/cR)$, with f and c indicating the frequency and speed of sound respectively.

The results, depicted in Fig. 4 (right), and any further presented acoustic results, are obtained at an upstream angle of 120° with respect to the trailing edge, as this matches the acoustic array of the experimental set-up from the Virginia Tech wind tunnel (see Fig. 2). This makes a comparison possible in later sections. The results in Fig. 4 (right) clearly show only marginal differences between the three numerical results, indicating proper scaling has been performed. In general, the spectra show no peak, indicating no strong shedding is present in the flow. The frequencies up to 2 kHz show a decreasing broadband noise signal.

To observe noise source locations in the near-field, a band pass filter is applied to the transient pressure data obtained from the LBM solution. Results for low and high frequencies are depicted in Fig. 5. Besides the acoustic pressure field, hydrodynamic pressure fluctuations can be observed in the boundary layer and in the wake. At both frequencies, the dominant noise comes from the trailing edge, where both pressure side and suction side boundary layer interact. As expected, the wavelength varies since specific frequencies are considered. At the high frequency, additional noise is present from the suction side transition strip.

VI. Comparison of different serrations

This section discusses the numerical acoustic results for the different serrations. Both the far-field noise reduction and the noise-source location are addressed. The numerical results are compared to the corre-

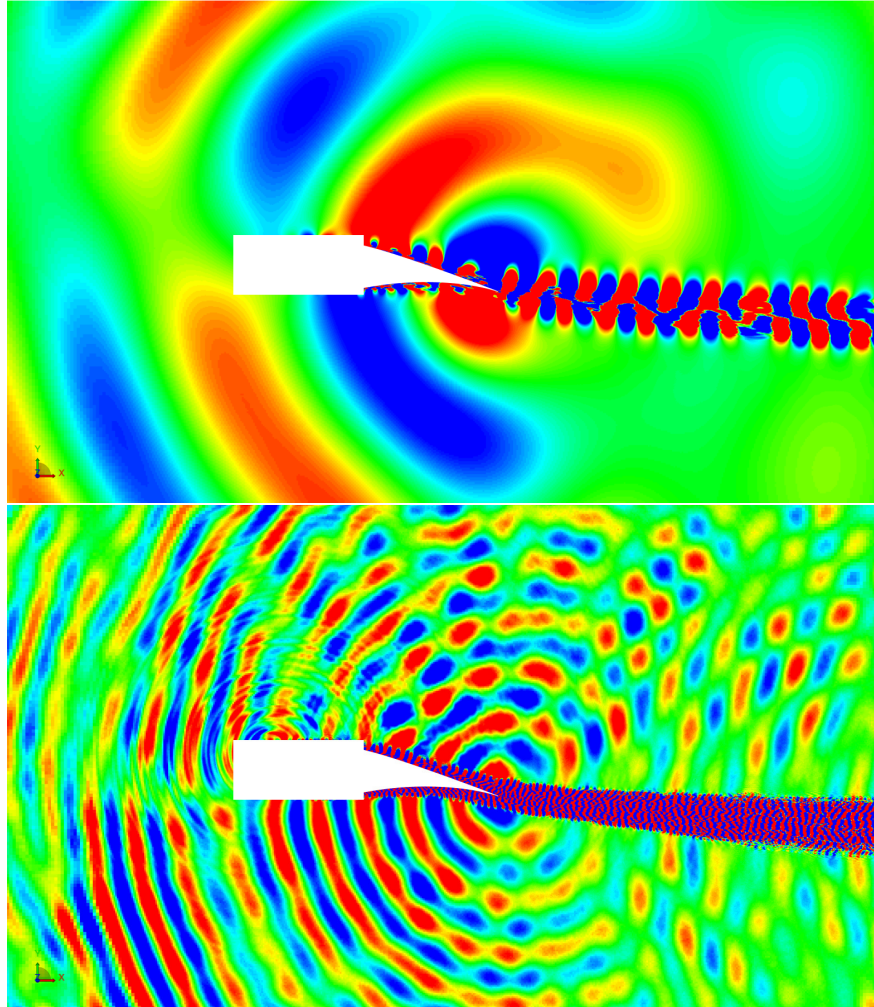


Figure 5. Instantaneous band passed pressure fields around the straight trailing edge model for $f_c = 400$ Hz (top) and $f_c = 1,000$ Hz (bottom).

sponding experimental results from the Virginia Tech wind tunnel.

A. Effect of a conventional serration

First, a comparison is made between the conventional serration and the straight trailing edge case. The serration effect is depicted in Fig. 6 for the design angle of attack. The trends found both for the numerical and experimental data are similar at low frequencies; reductions up to 5 dB are found. Larger discrepancies are noted above mid frequencies, but trends stay similar between both. In general, it can be concluded that this serration enhances noise reduction at low frequencies, while slightly increasing far-field noise levels at high frequencies.

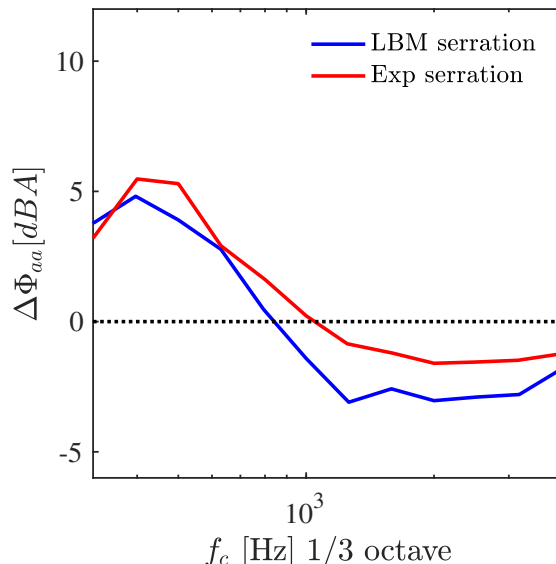


Figure 6. Reduction of far-field noise with respect to the straight edge due to the installation of the serrations. Positive is noise reduction.

B. Effect of a combed serration

In a similar fashion, the combed serration can be analyzed. Both experimental and numerical data are shown in Fig. 7. The results indicate the larger noise reductions obtained with the improved serrated geometry. The reduction is almost doubled. The numerical results indicate that noise reductions are observed at low frequencies while a noise increase is observed at high frequencies. Similar trends and levels (on average 2 dBA lower) are found for the experimental data, giving confidence in the numerically obtained far-field noise levels. A grid refinement study would be recommended to see if the numerical result converges towards the experimental data.

C. Comparison between a conventional and combed serration

A final comparison between both serrations is made by looking at the enhanced acoustic emission of the combed serration with respect to the conventional serration. The results in Fig. 8 indicate that a substantial increase in noise reduction is observed at the low frequencies for the combed serration. Although the reductions are about 1 – 3 dBA off, the trends are similar between LBM and experiment. This difference is likely caused by the slight underprediction of the far-field noise of the conventional serration, and the slight overprediction of the combed serration. It would be essential for future studies to see if, by improving the numerical setup, the variation can be reduced.

D. Directivity effects

The far-field results presented before were considered only the 120° direction, corresponding to the array location in the experiments. To study directivity effects, 360 virtual microphones were placed in a circle

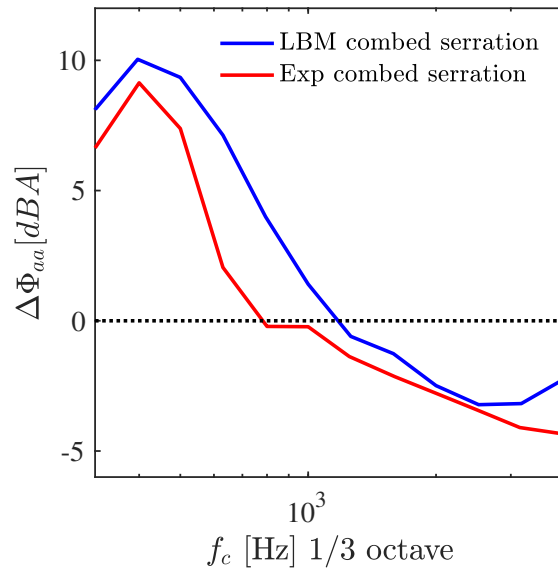


Figure 7. Reduction of far-field noise with respect to the straight edge due to the installation of the combed serrations. Positive is noise reduction.

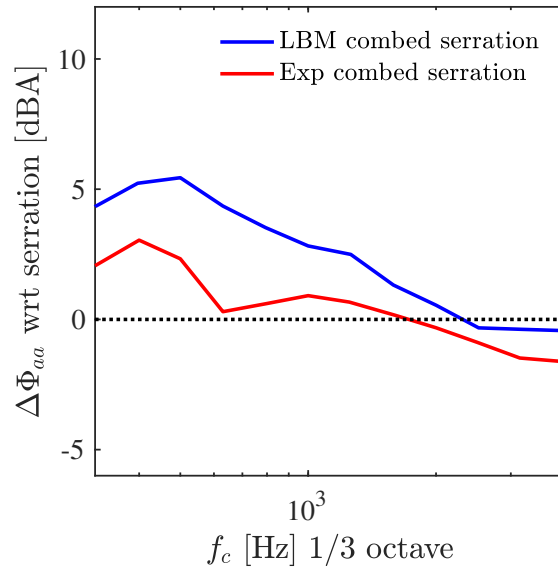


Figure 8. Reduction of far-field noise with respect to the conventional serrations due to the installation of the combed serrations. Positive is noise reduction.

of $10l$ diameter at mid-span with respect to the airfoil. Far-field noise levels are derived from the FW-H integral solution method for the straight, serrated and combed serrated case, and results are plotted for three different frequency bands in Fig. 9.

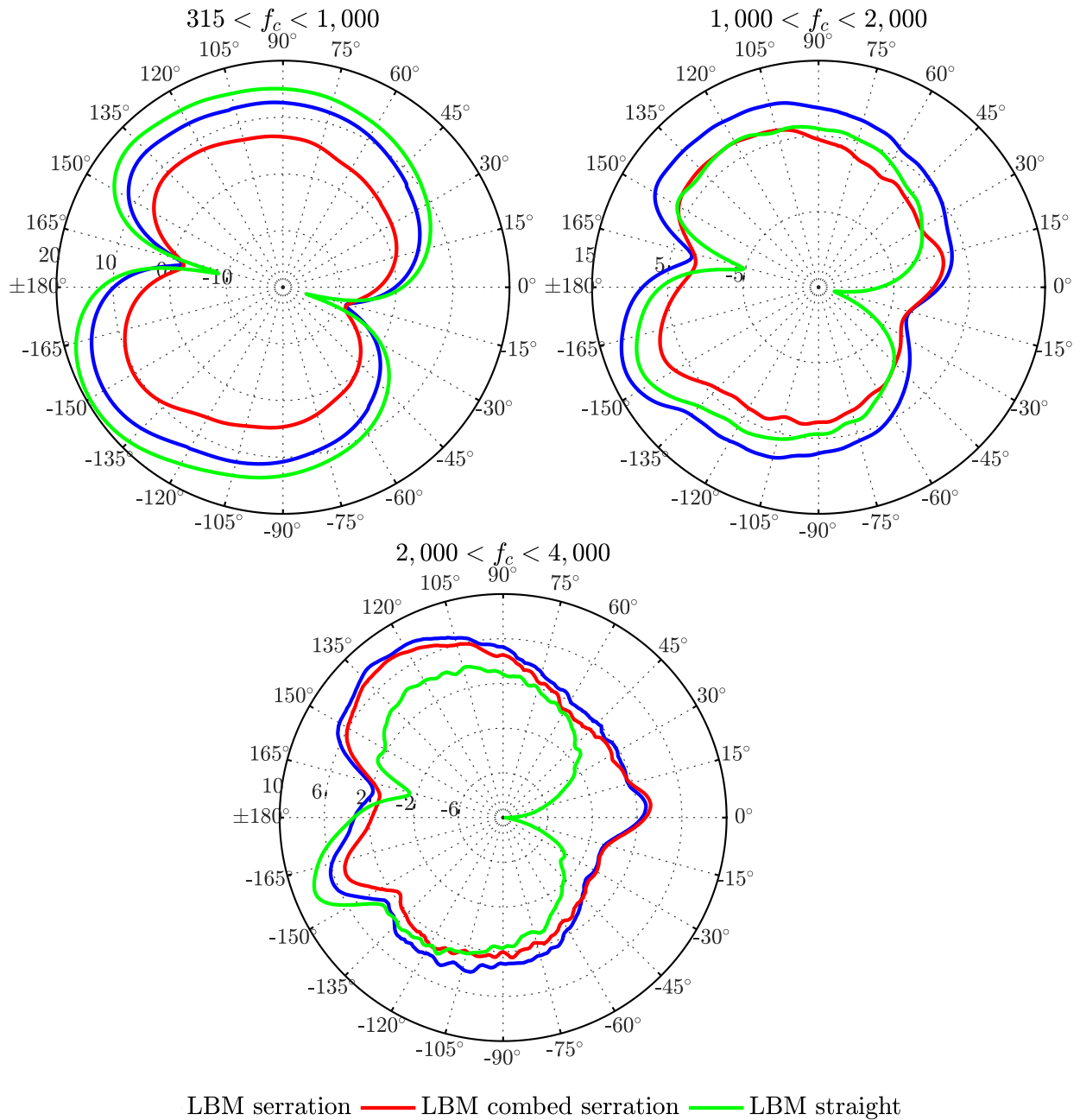


Figure 9. Far-field directivity (in dB), depicted in normalized acoustic pressure, for three frequency regimes

At low frequencies, a compact dipole source is observed. For increasing frequency, an asymmetric dipole directed towards the leading edge is obtained due to the phase shift of the acoustic pressure on the suction and pressure sides.⁴¹ The acoustic waves from both airfoil sides destructively interfere upstream of the leading edge, thus creating a zone of silence. At the highest frequency, a non-compact behavior is observed. At low frequencies, noise reduction is observed in all directions for both the conventional and combed serration, with the largest reduction at upstream angles between $120 - 150$ degrees. At mid frequencies, the conventional serrated edge starts producing more noise than the straight trailing edge case, while at the highest frequency, noise increases are observed for both cases in most directions. Results indicate that the upstream traveling

waves are most effectively canceled out using serrations, which affects the directivity pattern.

E. Flow induced noise detection

The flow induced noise detection tool can, as explained in the methodology, show whether or not co-rotating vortex pairs are reduced around the serrated trailing edges. If those vortex pairs are reduced, acoustic quadrupole sources are reduced, potentially reducing part of the trailing edge noise. Fig. 10 summarizes the results for both conventional and combed cases. A low and high center frequency were selected, where for both frequencies, the combed serration is quieter in the far field.

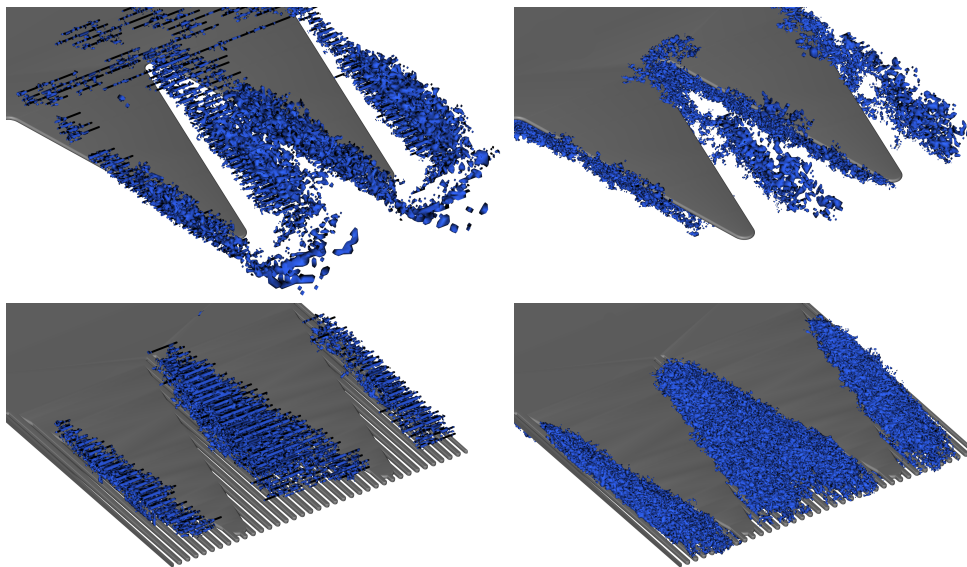


Figure 10. Iso-surfaces of co-rotating vortex pairs according to Powell’s analogy, for both the serrated (top) and combed serrated (bottom) design. On the left side, results are depicted at $f_c = 400$ Hz, right at $f_c = 1,000$ Hz.

At low frequency, the majority of the sources for the conventional serrated design are located between the teeth near the standing vortex, which is created due to the difference in pressure between the pressure and suction side. It develops into a larger horseshoe vortex further downstream. This vortex is, as expected, most dominant for the conventional serration. For the combed serration, this vortex is not visible, but more spread out in between the comb filaments. At increasing frequencies, the sources are moving from the location of the horseshoe in between the teeth, towards local edge noise, mainly at the pressure side of the serrated edge. Even though a large amount of vortex pairs is present near the combs, the far-field levels are lower for this configuration at both frequencies. A possible explanation may be that the combs scatter noise less efficiently than the tooth edges, or that the combs dissipate part of the acoustic energy.

VII. Conclusions and recommendations

The flow field and noise emission around a wind turbine airfoil with conventional and combed serrations were determined at chord based Reynolds numbers of 3.3 million. The flow and pressure fields were analyzed by evaluating the fully explicit, transient, compressible Lattice Boltzmann equation. Acoustic perturbations were directly obtained in the numerical domain, while the far field acoustic data was obtained by means of a FW-H and Curle integral solution. The numerical results were compared against acoustic array data obtained from wind tunnel campaigns performed in an anechoic wind tunnel.

The mean pressure distribution showed that experiment and simulation yield similar flow conditions. The three different acoustic post-processing methods were compared for the straight edge case. Only marginal differences were present, giving confidence to the numerical results.

Next, noise reductions were determined due to the installation of serrations. Both the numerical results and the experiments showed that serrations reduce noise in the low frequency regime, while noise increases are found at high frequencies. The largest reductions were found at upstream angles, between $120^\circ - 150^\circ$,

where also the experimental array was located. The numerical results also reproduced the experimental finding that combed serrations are quieter than standard serrations.

The trends for experiment and simulation were similar, giving confidence in the results obtained from the LBM solver. However, the peak reduction was sometimes underpredicted (e.g. conventional serration) but also overpredicted (combed serration). In future studies, it is essential to test multiple grids, as well as different simulation times. Especially the low frequency noise results considered here may be dependent on enough acoustical data.

References

- ¹van den Berg, F., Pedersen, E., Bouma, J., and Bakker, R., “Windfarm perception: Visual and acoustic impact of wind turbine farms on residents,” Tech. rep., University of Groningen, 2008.
- ²Maris, E., Stallen, P., Vermunt, R., and Steensma, H., “Noise within the social context: Annoyance reduction through fair procedures,” *Journal of the Acoustical Society of America*, Vol. 121, No. 4, 2007, pp. 2000–2010.
- ³Howe, B., Gastmeier, B., and McCabe, N., “Wind Turbines and Sound: Review and Best Practice Guidelines,” *Canadian Wind Energy Association*, 2007.
- ⁴Leventhall, G. and Bowdler, D., *Wind Turbine Noise: How it is produced, propagated measured and received*, MultiScience, 2011.
- ⁵Oerlemans, S., “Reduction of wind turbine noise using blade trailing edge devices,” *22nd AIAA/CEAS Aeroacoustics Conference*, , No. 3018, 2016.
- ⁶Brooks, T., Pope, D., and Marcolini, M., “Airfoil self-noise and prediction,” Tech. rep., NASA Reference Publication 1218, 1989.
- ⁷Blake, W., *Mechanics of flow-induced sound and vibration, volumes I and II*, Academic Press, 1986.
- ⁸Oerlemans, S., Sijtsma, P., and Lopez, B. M., “Reduction of wind turbine noise using optimized airfoils and trailing-edge serrations,” *AIAA Journal*, Vol. 47, 2009, pp. 1470–1481.
- ⁹Moreau, D. and Doolan, C., “Noise-Reduction Mechanism of a Flat-Plate Serrated Trailing Edge,” *AIAA Journal*, Vol. 51, 2013, pp. 2513–22.
- ¹⁰Chong, T. and Joseph, P., “Airfoil self noise reduction by non-flat plate type trailing edge serrations,” *Applied Acoustics*, Vol. 74, 2013, pp. 607–13.
- ¹¹Arce-León, C., Ragni, D., Pröbsting, S., Scarano, F., and Madsen, J., “Flow topology and acoustic emissions of trailing edge serrations at incidence,” *Experiments in Fluids*, Vol. 57, No. 91, 2016.
- ¹²Dassen, A., Parchen, R., Bruggeman, J., and Hagg, F., “Results of a wind tunnel study on the reduction of airfoil self-noise by the application of serrated blade trailing edges,” *Proceeding of the European Union Wind Energy Conference and Exhibition*, 1996, pp. 800–803.
- ¹³Gruber, M., Joseph, P., and Chong, T., “On the mechanisms of serrated airfoil trailing edge noise reduction,” *17th AIAA/CEAS Aeroacoustic Conference*, , No. 2781, 2011, pp. 1–23.
- ¹⁴Avallone, F., Pröbsting, S., and Ragni, D., “Three-dimensional flow field over a trailing-edge serration and implications on broadband noise,” *Physics of Fluids*, Vol. 28, 2016, pp. 1–20.
- ¹⁵Gruber, M., *Airfoil noise reduction by edge treatments*, Ph.D. thesis, University of Southampton, 2012.
- ¹⁶Howe, M., “Aerodynamic noise of a serrated trailing edge,” *Journal of Fluids and Structures*, Vol. 5, 1991, pp. 33–45.
- ¹⁷Howe, M., “Noise produced by a sawtooth trailing edge,” *Journal of the Acoustical Society of America*, Vol. 90, 1991, pp. 482–7.
- ¹⁸Chong, T. and Vathylakis, A., “On the aeroacoustic and flow structures developed on a flat plate with a serrated sawtooth trailing edge,” *Journal of Sound and Vibration*, Vol. 354, 2015, pp. 65–90.
- ¹⁹Jones, L. and Sandberg, R., “Acoustic and hydrodynamic analysis of the flow around an aerofoil with trailing edge serrations,” *Journal of Fluid Mechanics*, Vol. 706, 2012, pp. 295–322.
- ²⁰van der Velden, W., van Zuijlen, A., and Ragni, D., “Flow topology and noise emission around straight, serrated and slitted trailing edges using the Lattice Boltzmann methodology,” *22nd AIAA/CEAS Aeroacoustics Conference*, , No. 3021, 2016.
- ²¹van der Velden, W. and Oerlemans, S., “Numerical analysis of noise reduction mechanisms on improved trailing edge serrations using the Lattice Boltzmann method,” *35th ASME Wind Energy Symposium*, 2017, pp. 1–15.
- ²²Ffowcs-Williams, J. and Hawkings, D., “Sound generation by turbulence and surfaces in arbitrary motion,” *Philosophical Transactions of the Royal Society of London*, Vol. 264, 1969, pp. 321–342.
- ²³Curle, N., “The influence of solid boundaries upon aerodynamic sound,” *Proceedings of the Royal Society of London*, Vol. 231, 1955, pp. 505–514.
- ²⁴van der Velden, W., Pröbsting, S., van Zuijlen, A., de Jong, A., Guan, Y., and Morris, S., “Numerical and experimental investigation of a beveled trailing-edge flow field and noise emission,” *Journal of Sound and Vibration*, Vol. 384, 2016, pp. 113–129.
- ²⁵Chen, H., Chen, S., and Matthaeus, W., “Recovery of the Navier-Stokes equations using a lattice-gas Boltzmann method,” *Physical Review*, Vol. 8, No. 5339-5342, 45.
- ²⁶Succi, S., *The lattice Boltzmann equation for fluid dynamics and beyond*, Oxford University Press, 2001.
- ²⁷van der Velden, W., *Computational aeroacoustic approaches for wind turbine blade noise prediction*, Ph.D. thesis, Delft University of Technology, 2017.

- ²⁸Bhatnagar, P., Gross, E., and Krook, M., "A model for collision processes in gases: Small amplitude processes in charged and neutral one-component systems," *Physical Review*, Vol. 94, No. 3, 1954, pp. 511–525.
- ²⁹Yakhot, V. and Orszag, S., "Renormalization group analysis of turbulence. I Basic theory," *Journal of Scientific Computing*, Vol. 1, No. 1, 1986, pp. 3–51.
- ³⁰Launder, B. and Spalding, D., "The numerical computation of turbulent flows," *Computer Methods in Applied Mechanics and Engineering*, Vol. 3, 1974, pp. 269–289.
- ³¹Bres, G., Perot, F., and Freed, D., "Properties of the Lattice-Boltzmann method for acoustics," *15th AIAA/CEAS Aeroacoustic Conference*, Vol. 3711, 2009, pp. 1–14.
- ³²Farassat, F. and Succi, G., "A review of propeller discrete frequency noise prediction technology with emphasis on two current methods for time domain calculations," *Journal of Sound and Vibration*, Vol. 71, No. 3, 1980, pp. 399–419.
- ³³Casalino, D., "An advanced time approach for acoustic analogy predictions," *Journal of Sound and Vibration*, Vol. 261, No. 4, 2003, pp. 583–612.
- ³⁴Powell, A., "Theory of vortex sound," *Journal of the Acoustical Society of America*, Vol. 36, No. 1, 1964, pp. 177–195.
- ³⁵Mann, A., Kim, M., Wu, J., Perot, F., Grilliat, J., Jacob, M., and Colman, M., "Airfoil Tip Leakage Aeroacoustics Predictions using a Lattice Boltzmann Based Method," *22nd AIAA/CEAS Aeroacoustics Conference*, , No. 2825, 2016, pp. 1–17.
- ³⁶Ffowcs-Williams, J., "Hydrodynamic Noise," *Annual Review of Fluid Mechanics*, Vol. 1, 1969, pp. 197–222.
- ³⁷Költzsch, P., *Strömungsmechanisch erzeugter Lärm*, Ph.D. thesis, Technische Universität Dresden, 1974.
- ³⁸Devenport W.J., Burdisso R.A., Borgoltz A., Ravetta P. and Barone M.F., "Aerodynamic and Acoustic Corrections for a Kevlar-Walled Anechoic Wind Tunnel," *16th AIAA/CEAS Aeracoustics Conference*, , No. 3749, 2010.
- ³⁹Oberai, A., Roknaldin, F., and Hughes, T., "Trailing edge noise due to turbulent flows," 02-002, Boston University, 2002.
- ⁴⁰Ewert, R. and Schröder, W., "On the simulation of trailing edge noise with a hybrid LES/APE method," *Journal of Sound and Vibration*, Vol. 270, 2004, pp. 509–524.
- ⁴¹Roger, M. and Moreau, S., "Extensions and limitations of analytical airfoil broadband noise models," *International Journal of Aeroacoustics*, Vol. 9, No. 3, 2010, pp. 273–305.